Representation of LSF and PSF for GDAAS-2

L. Lindegren

GAIA–LL–046 (2 May 2003)

Abstract. A parametrisation of the quasi-monochromatic line-spread function (LSF) for GAIA is proposed, using an analytical function describing the diffraction wings plus a 'bi-quartic' spline representation of the core. The quasi-monochromatic point-spread function (PSF) is modelled as the product of the along-scan and across-scan LSFs. Two appendices give details on the numerical PSF calculation and on bi-quartic B-splines.

1 Introduction

For the improved instrument modelling in GDAAS-2 (see GAIA-LL-044, V.4) it is necessary to represent the quasi-monochromatic line-spread functions (LSF) in the Astro and Spectro instruments of GAIA by means of continuous functions depending on a finite number of parameters. The values of these parameters are (completely or partially) determined as part of the instrument calibration process.

For some algorithms, notably the processing of overlapping images (for double stars and in photometry), it is also necessary to define similarly parameterised two-dimensional functions, i.e. the point-spread functions (PSF). However, as a first approximation, sufficient for GDAAS-2, the quasi-monochromatic PSF could be written as the product of the along-scan LSF with an across-scan LSF which is assumed to be known (thus not calibrated).

Several issues relevant for the LSF/PSF representation are discussed in this note: the numerical calculation of the PSF, the intensity distribution in the wings, how well the PSF is described by the LSF product, and a possible parametrisation. The main result is that a general representation of the along- and across-scan LSFs in Astro is proposed, which may be used in GDAAS-2, and which should be readily extendable to Spectro. However, it should be noted that the representation is probably not good enough for the real GAIA data processing.

All PSF calculations are based on GAIA-2 parameters except the wavefront error (WFE) maps, which are scaled versions of the old ones. A consistent recalculation of PSFs should be made once a representative set WFE maps for GAIA-2 is available.

2 Definitions

The *optical point spread function*, denoted $P^O(u, v)$, describes the instantaneous distribution of intensity (per solid angle) in the focal plane. Here, u and v are the angular

coordinates along and across scan, respectively, relative to the image centroid, and measured in radians or pixels. The optical PSF may refer to a single wavelength (λ), to a limited wavelength interval (e.g. as defined by BBP filter band m), or as integrated over the whole Astro spectral region (no filter). These different versions of the optical PSF are distinguished by the use of subscripts λ, m or 0. In either case the optical PSF is by definition normalised: $\iint P^O(u,v)\,\mathrm{d}u\,\mathrm{d}v = 1$.

The optical PSF is not directly observable in GAIA. What is observed (and calibrated) is a smoothed-out version which we model as the convolution of P^O with a kernel $K(u,v)$ representing integration over the pixel area, motion of the optical PSF relative to the charge image, electronic cross-talk, etc. The result may be referred to as the *total PSF* and denoted $P(u,v)$. Subscripts λ, m or 0 are used with the same meaning as for the optical PSF. The total PSF is also normalised: $\iint P(u,v)\,\mathrm{d}u\,\mathrm{d}v = 1$.

The *along-scan line spread function* is the marginal density of P on the u axis: $L(u) = \int P(u,v)\,\mathrm{d}v$. Similarly, the *across-scan line spread function* is the marginal density on the v axis: $C(v) = \int P(u,v)\,\mathrm{d}u$. From the normalisation of P it follows that $\int L(u)\,\mathrm{d}u = \int C(v)\,\mathrm{d}v = 1$. Superscript ^{O} and subscripts λ, m or 0 can be added to these functions with the same meanings as for P.

3 Decomposition of the PSF

In the absence of aberrations the monochromatic optical PSF is, according to Eq. (8),

$$P^O_\lambda(u,v) = \frac{DH}{\lambda^2}\,\mathrm{sinc}^2(\pi u D/\lambda)\,\mathrm{sinc}^2(\pi v H/\lambda) \tag{1}$$

(where $\mathrm{sinc}\,x = \sin x/x$) from which

$$L^O_\lambda(u) = \frac{D}{\lambda}\,\mathrm{sinc}^2(\pi u D/\lambda)\,, \qquad C^O_\lambda(v) = \frac{H}{\lambda}\,\mathrm{sinc}^2(\pi v h/\lambda) \tag{2}$$

Consequently, it is in this case possible to decompose the PSF as the product of the along- and across-scan LSFs:

$$P^O_\lambda(u,v) = L^O_\lambda(u)\,C^O_\lambda(v) \tag{3}$$

If the kernel can be written $K(u,v) = K_1(u)K_2(v)$ (which is the case for the present model, cf. Appendix A), then it follows that the total PSF can be similarly decomposed:

$$P_\lambda(u,v) = L_\lambda(u)\,C_\lambda(v) \tag{4}$$

Such a decomposition does however *not* hold (strictly) for the polychromatic PSFs (P_m and P_0), although it may be a good approximation in the quasi-monochromatic case (P_m). Nor does it hold in the presence of aberrations. However, to a certain approximation we may of course *assume* that

$$P_m(u,v) \simeq L_m(u)\,C_m(v) \tag{5}$$

in the aberrated, quasi-monochromatic case. The validity of this approximation, proposed for GDAAS-2, is illustrated in Figs. 1 and 2.

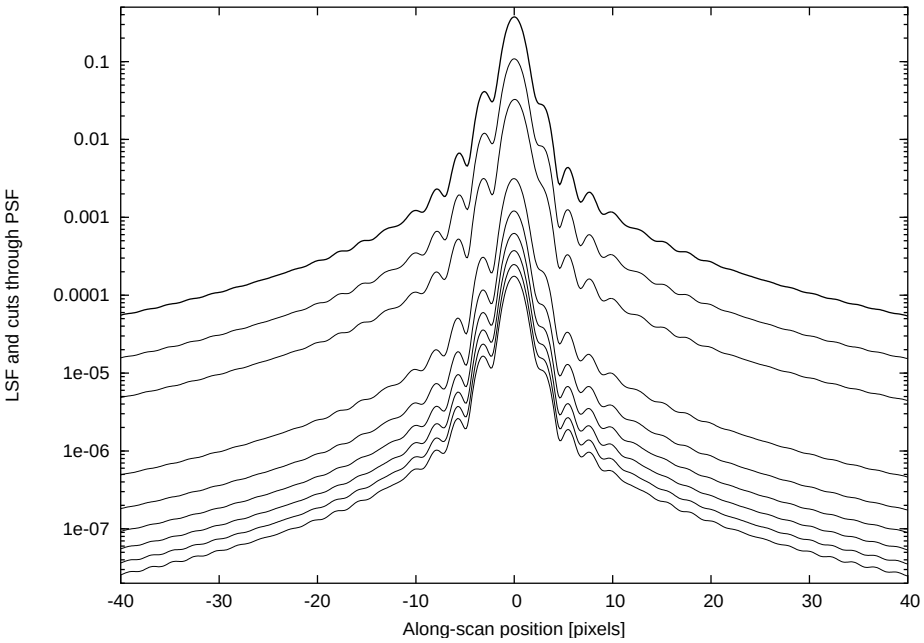

FIGURE 1: The LSF (heavy curve) and 8 different cuts through the PSF (at $v = 0, 2, \ldots, 14$ pixels from the centroid). The PSF was computed for BBP band B67 and a representative WFE map, with rms WFE 38 nm. The general similarity of the LSF and the different cuts suggests the approximate validity of the PSF decomposition in (5).

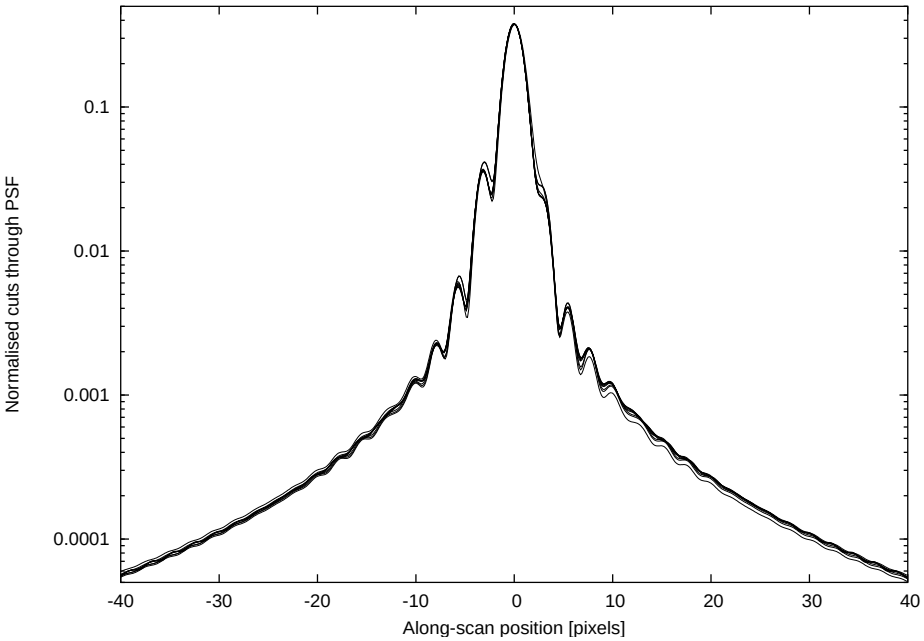

FIGURE 2: Same curves as in Fig. 1 but normalised to unit area.

4 The wings of the LSF

The monochromatic optical LSFs in (2) contain an infinite number of zeroes (at $u = n\lambda/D$ for integer $n \neq 0$) due to destructive interference. For a finite bandwidth $\Delta\lambda$ the intensity oscillations disappear for angles exceeding $\sim \lambda_{\rm eff}^2/\Delta\lambda D$, or some 10 pixels away for a broad-band system ($\lambda_{\rm eff}/\Delta\lambda \sim 5$). In the wings of the LSF the intensity can therefore be estimated by putting $\sin^2(\pi u D/\lambda) \simeq 0.5$ in (2), yielding:

$$L_m^O(u) \simeq \frac{\lambda_m}{2\pi^2 D u^2}\,, \qquad C_m^O(v) \simeq \frac{\lambda_m}{2\pi^2 H v^2} \tag{6}$$

where λ_m is the effective wavelength in band m. These expressions hold to good accuracy also for the total LSFs, since the wings are very wide compared with the kernel function K. But what about aberrations?

In Figs. 3–7 the total LSFs for several representative WFE maps are superposed on a logarithmic intensity scale. Whereas the inner part of the LSFs differ a lot because of the different aberrations, it is seen that the wings are quite similar and rather well represented by the aberration-free curve. This suggests that, as a first approximation, the wings of the LSF can be regarded as known and given by (6).

5 Representation of the LSF core

While the outer parts (wings) of the LSFs may be approximated as described above, the inner parts need a very general and flexible representation for calibration (and simulation) purposes. Cubic splines have been proposed for this purpose, using equidistant knots separated by exactly one pixel. Such a spline function $f(u)$ has the interesting property that $\sum_j f(jp_u - u_0)$ is invariant with respect to u_0 (p_u is the along-scan pixel size). Numerical experiments indicate that the fitted LSF should have this property in order to avoid estimation biases as function of sub-pixel position.

From the present PSF/LSF calculations it was however found that the one-pixel knot separation is insufficient for fitting a cubic spline at the shortest wavelengths. The knot separation had to be reduced to about 0.6 pixel in order to get a satisfactory fit. But such a spline would not satisfy the invariance condition mentioned above. Using a higher-order spline (on a one-pixel grid) would not improve the fit much either.

After some experimentation, an apparently satisfactory solution was found by means of a variant of quartic spline defined on a half-pixel grid but still respecting the invariance condition above. It can be thought of as a conventional cubic spline, defined on a half-pixel grid, but convolved with a rectangular function of a full pixel width. The last convolution obviously guarantees the invariance condition, while the half-pixel grid gives sufficient flexibility even for the shortest wavelength. This 'bi-quartic' spline is further described in Appendix B, which also contains an efficient algorithm for computing the corresponding B-spline coefficients.

Figures 9–13 show examples of quasi-monochromatic along-scan LSFs with fitted bi-quartic splines.

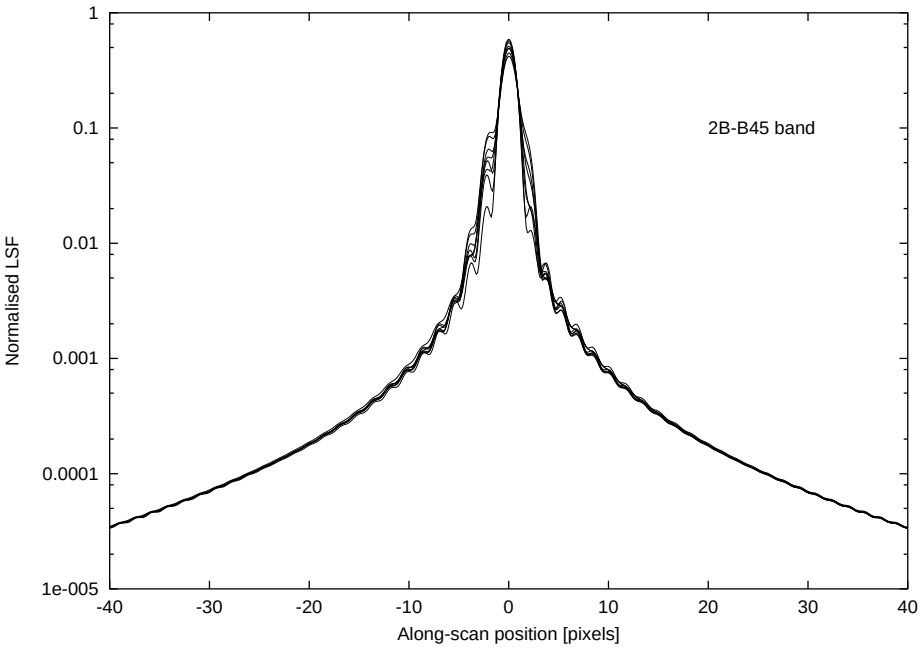

FIGURE 3: The LSF in band 2B-B45 for eight different WFE maps (with rms WFE ranging from 0 to 42 nm excluding piston and tilt).

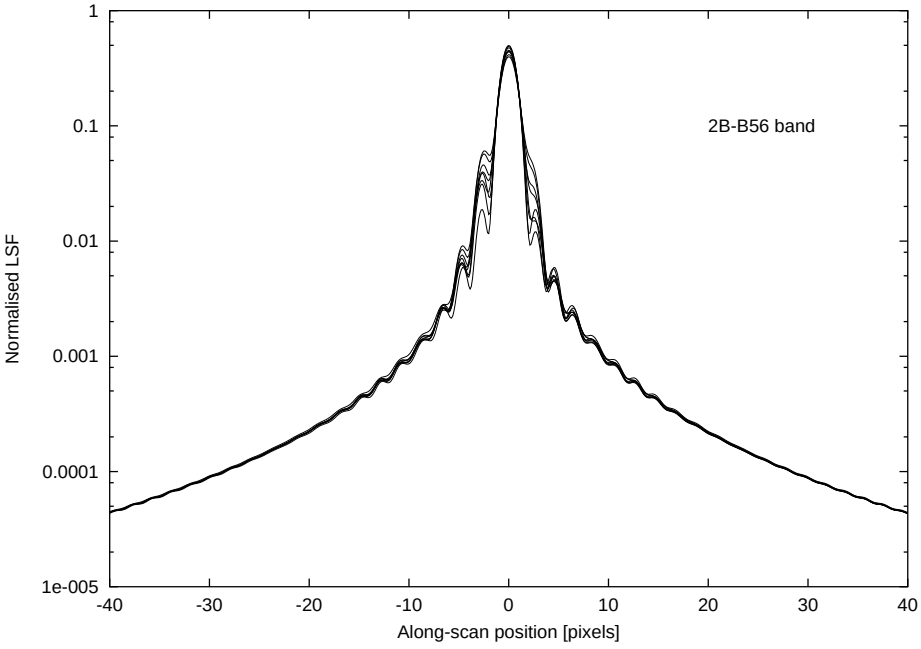

FIGURE 4: The LSF in band 2B-B56 for the same WFE maps as in Fig. 3.

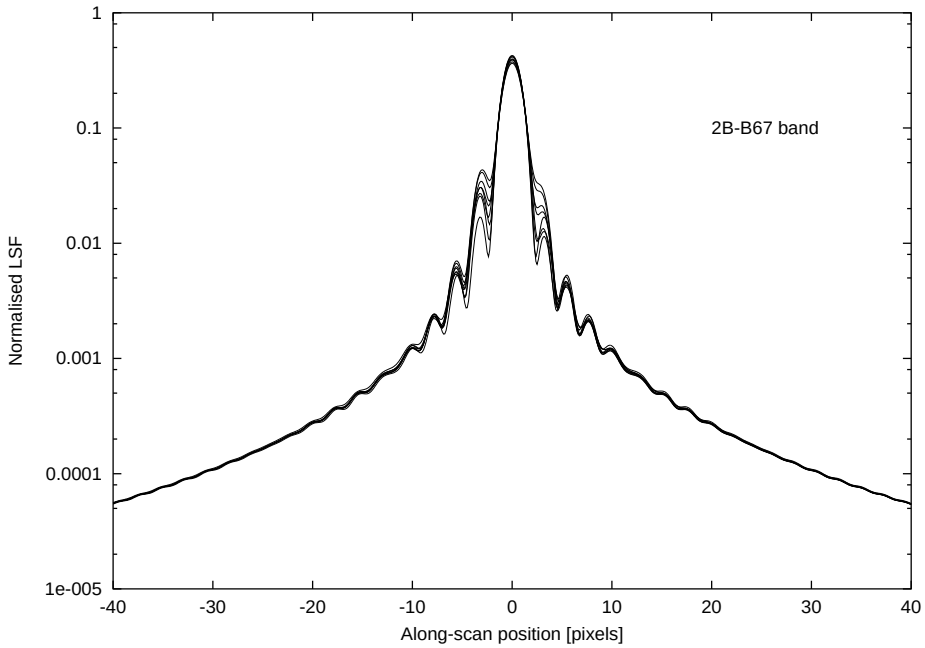

FIGURE 5: The LSF in band 2B-B67 for the same WFE maps as in Fig. 3.

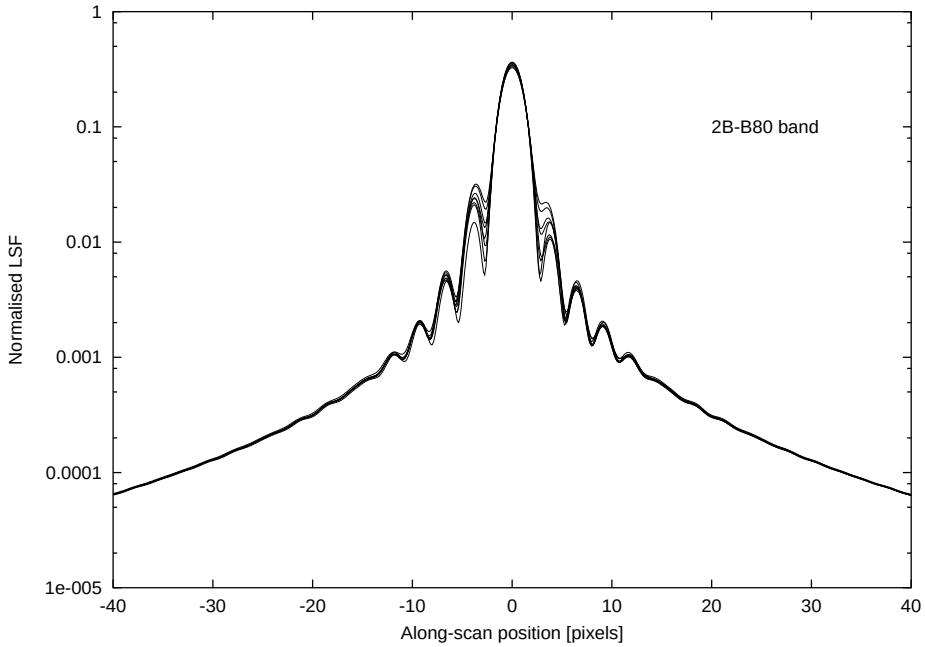

FIGURE 6: The LSF in band 2B-B80 for the same WFE maps as in Fig. 3.

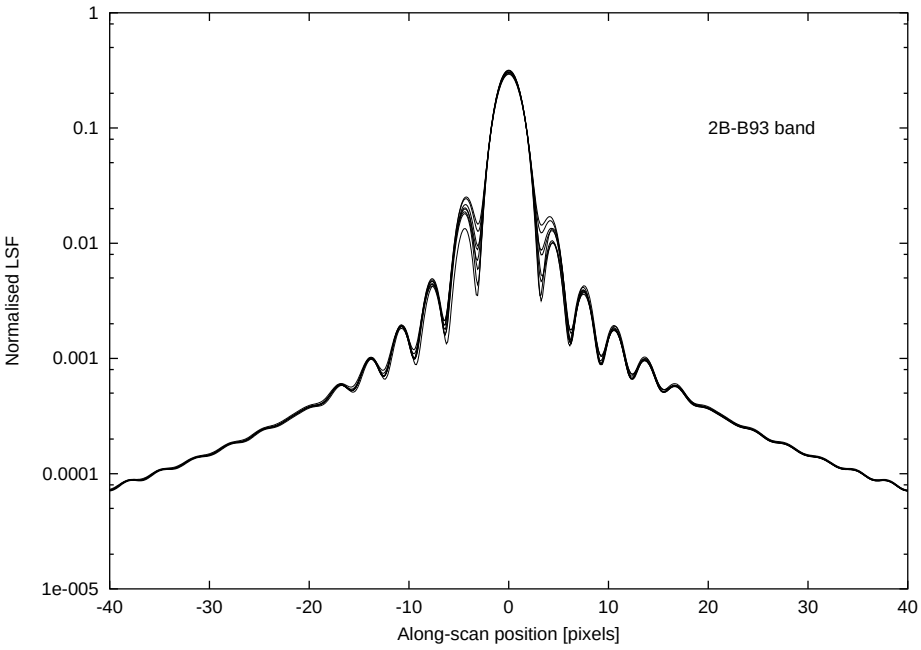

FIGURE 7: The LSF in band 2B-B93 for the same WFE maps as in Fig. 3.

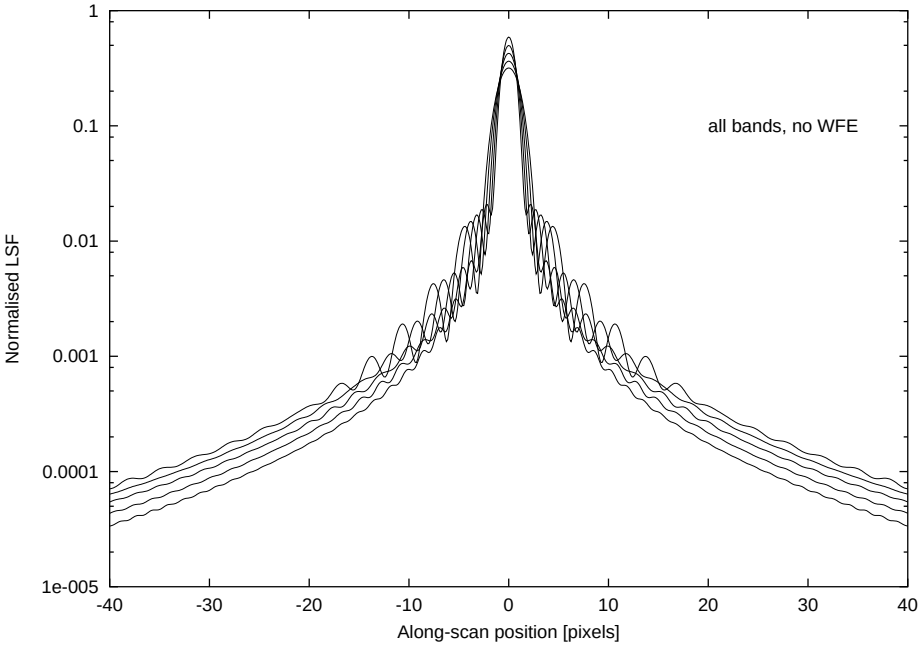

FIGURE 8: The LSF without aberrations for the five bands in system 2B.

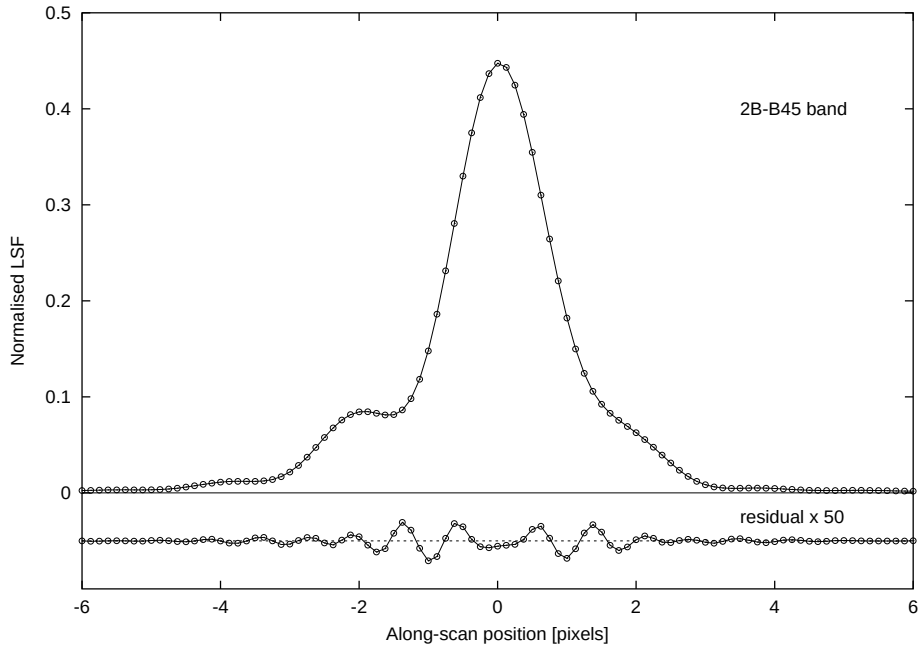

FIGURE 9: Bi-quartic spline fit to the LSF in band 2B-B45 for a representative WFE map. The residuals of the fit, magnified 50 times, are shown in the lower panel.

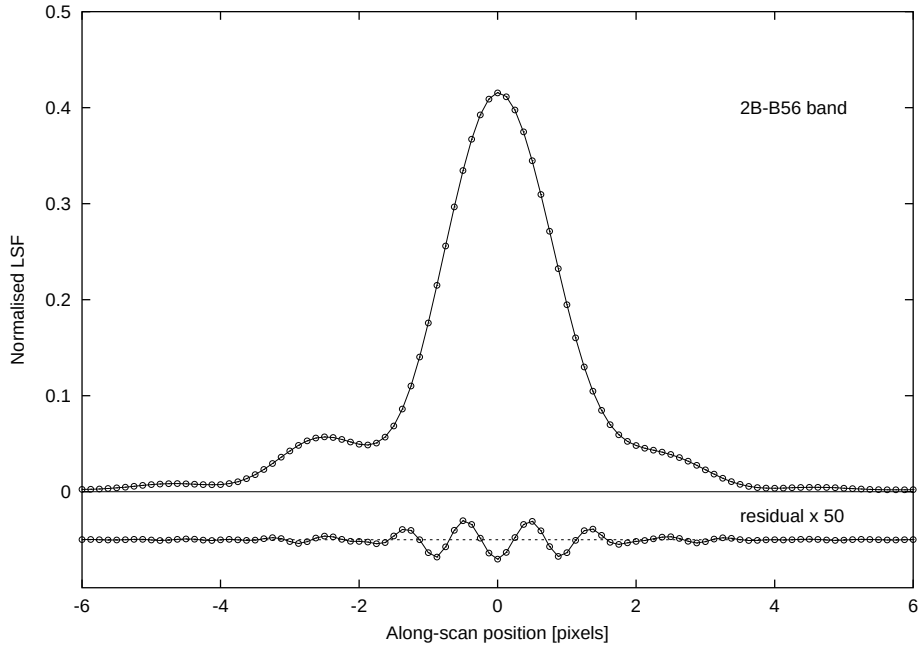

FIGURE 10: Bi-quartic spline fit to the LSF in band 2B-B56 for the same WFE map as in Fig. 9.

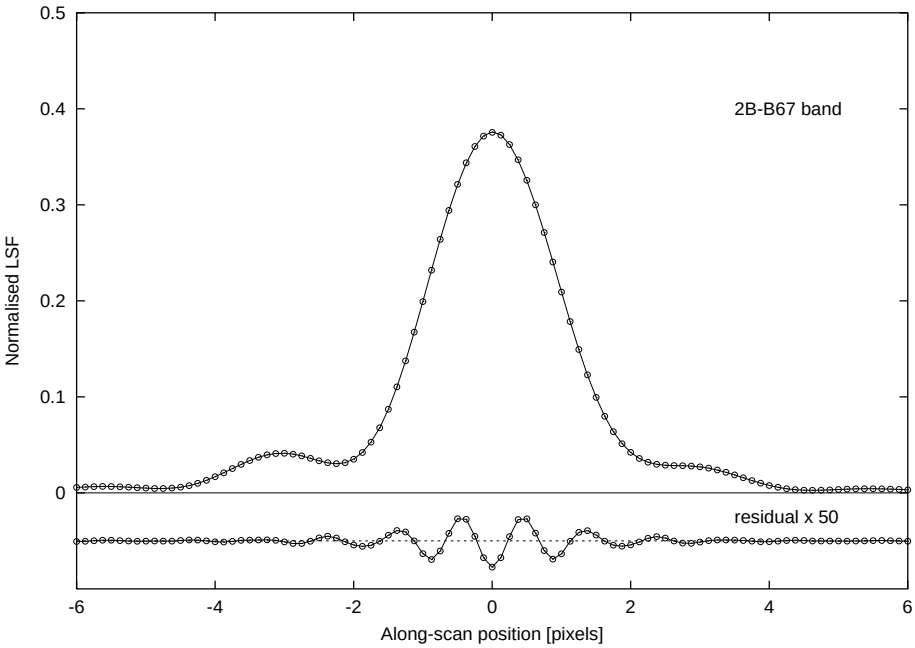

FIGURE 11: Bi-quartic spline fit to the LSF in band 2B-B67 for the same WFE map as in Fig. 9.

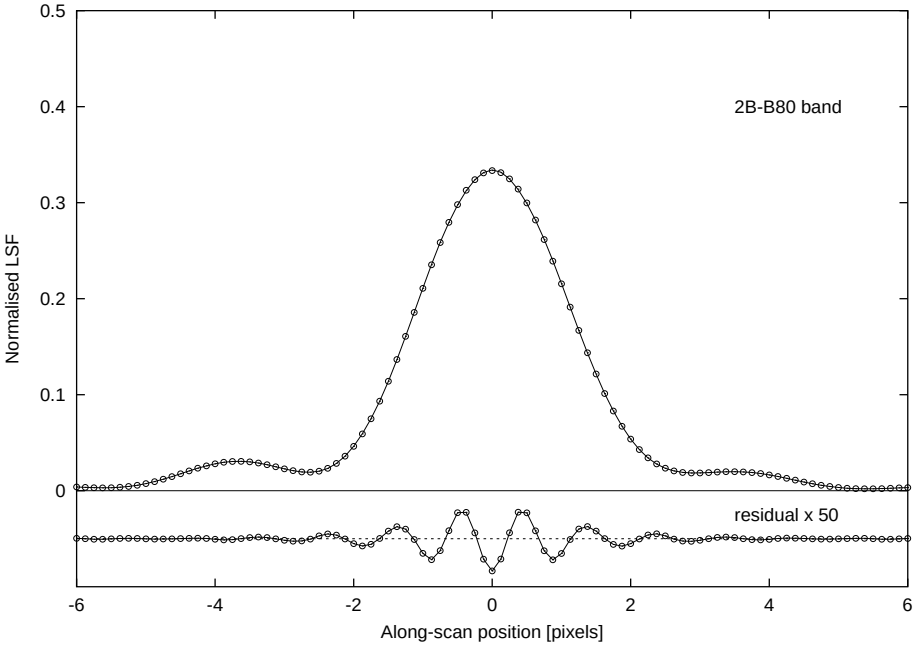

FIGURE 12: Bi-quartic spline fit to the LSF in band 2B-B80 for the same WFE map as in Fig. 9.

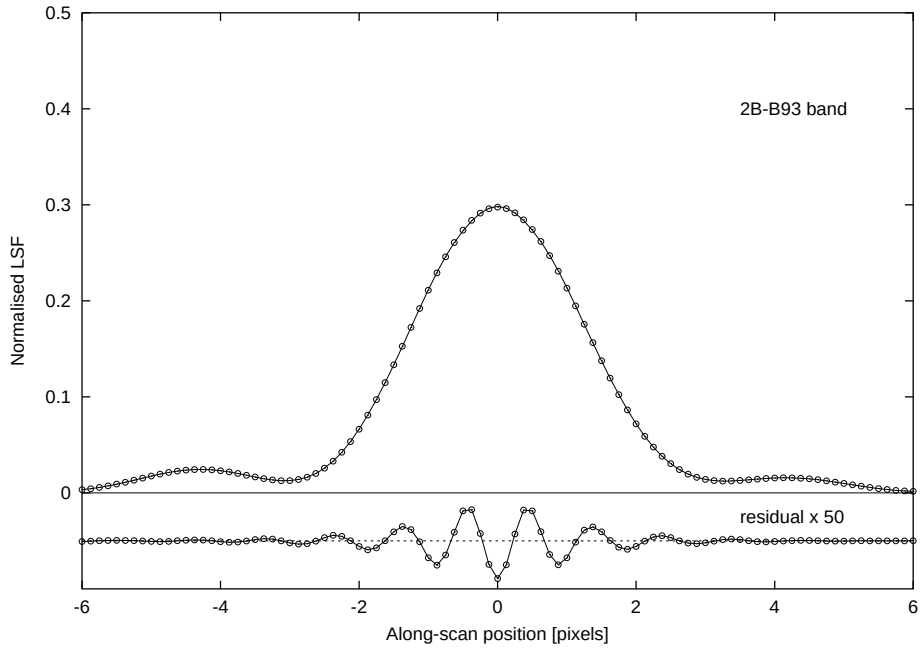

FIGURE 13: Bi-quartic spline fit to the LSF in band 2B-B93 for the same WFE map as in Fig. 9.

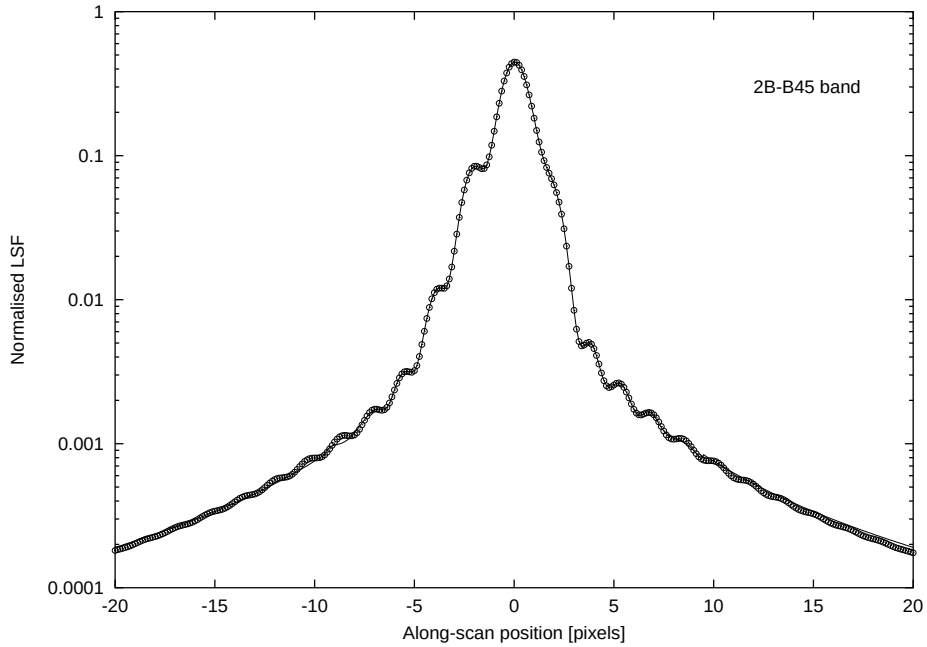

FIGURE 14: The fit in Fig. 9 on a logarithmic intensity scale, including the wings represented by the Cauchy function.

6 Proposed LSF/PSF representation for GDAAS-2

Based on the various considerations above, we may arrive at the following fairly general, parametrised LSF representation:

$$L_m(u) = \frac{a_0}{1 + [(u - a_1)/a_2]^2} + \sum_{k=1}^{n} b_k B_k(u) \tag{7}$$

(and similarly for $C_m(v)$), where the B-splines $B_k(u)$ are defined on the grid $u_k = u_0 + k\delta u$ (with u measured in pixels). The first term in (7) represents the wings of the LSF by means of a Cauchy distribution, which reduces to (6) sufficiently far from the core; to this is added the spline representation of the core, which may be non-zero in $[u_{-2}, u_{n+2}]$. Figure 14 shows a fit including the wings in (7).

The complete specification of a LSF thus requires $n + 5$ numbers, viz.:

1. the grid spacing δu $(= 0.5)$, in pixels
2. the coordinate origin u_0, in pixels
3. the n B-spline coefficients b_k, $k = 1 \ldots n$
4. the wing profile height a_0
5. the wing centre coordinate a_1
6. the wing half-width a_2

n, Δu and a_2 are fixed by convention (n should be roughy twice the number of pixels over which the core may be fitted). u_0 is fixed by the adopted convention for the definition of the centroid (e.g. the 'minimum difference mirror point'; GAIA–LL–044 [V.4], footnote 10). a_1 must in practice be adjusted to the centroid position ($a_1 = 0$). Finally the sum of b_k is constrained by the normalisation condition $\int L_m(u)\,\mathrm{d}u = \pi a_0 a_2 + \sum_{k=1}^{n} b_k = 1$.

With a similar parametrisation of the across-scan LSF $C_m(v)$, the quasi-monochromatic PSF follows from (5).

Appendix A: Numerical calculation of PSF

The numerical calculation of the PSF and LSF was discussed in SAG–LL–016, 024, 025 and GAIA–LL–039. The relevant and updated equations are repeated here. Let (x, y) be linear coordinates in the pupil plane [m] and (u, v) the corresponding angular coordinates in the image plane [rad]. x and u are along-scan; y and v across-scan. For the WFE map $w(x, y)$ the normalised monochromatic optical PSF is

$$P_\lambda^O(u, v) = \frac{1}{\lambda^2 DH} \left| \iint_{-\infty}^{+\infty} A(x, y) \exp[ik(xu + yv)]\,\mathrm{d}x\,\mathrm{d}y \right|^2 \tag{8}$$

where λ is wavelength, $k = 2\pi/\lambda$ the wavenumber, D and H the pupil dimensions along x and y, and A the complex amplitude of the incident wavefront in the pupil plane:

$$A(x,y) = \begin{cases} \exp[ikw(x,y)] & \text{for } (x,y) \in \text{pupil} \\ 0 & \text{otherwise} \end{cases} \tag{9}$$

Equation (8) is normalised such that $\iint P_\lambda^O(u,v) = 1$.

The double integral in (8) is approximated by a discrete Fourier transform (DFT), computed by the FFT algorithm. The algorithm used (`DFFT` from Netlib) computes one- or multi-dimensional DFTs, in the present two-dimensional case defined by the double sum

$$F(j_u, j_v) = \sum_{j_x=1}^{N_x} \sum_{j_y=1}^{N_y} A(j_x, j_y) \exp\left[si2\pi\left(\frac{(j_x-1)(j_u-1)}{N_x} + \frac{(j_y-1)(j_v-1)}{N_y}\right)\right] \tag{10}$$

for $j_u = 1 \ldots N_x$, $j_v = 1 \ldots N_y$, where $s = \pm 1$. The matrix A represents the pupil function (9) with the coordinate mapping $x = (j_x - 1)\Delta x$ for $j_x \le N_x/2$ and $x = (j_x - 1 - N_x)\Delta x$ for $j_x > N_x/2$ (and similarly for y). In the image plane the mapping is $u = (j_u - 1)\Delta u$ for $j_u \le N_x/2$ and $u = (j_u - 1 - N_x)\Delta u$ for $j_u > N_x/2$ (and similarly for v). Comparing (10) with (8) it is seen that the double integral is approximated by $F(j_u, j_v)\Delta x \Delta y$ provided that $N_x \Delta x \Delta u = \lambda$ and $N_y \Delta y \Delta v = \lambda$. The image must be computed on a sub-pixel grid, say with a sampling distance of $s_u = s_v = 1/8$ pixel in each coordinate. Let $p_u \times p_v$ be the pixel size (in radians); then $\Delta u = s_u p_u$ and $\Delta v = s_v p_v$ and consequently, for fixed N_x and N_y,

$$\Delta x = \frac{\lambda}{N_x s_u p_u}, \qquad \Delta y = \frac{\lambda}{N_y s_v p_v} \tag{11}$$

For the numerical calculation we are basically free to choose the sampling steps s_u, s_v (in pixels) and the number of discretisation points N_x, N_y. However, the choices should be guided by the required properties of the computed PSF. For instance, s_u and s_v must be small enough to sample the image at least up to the Nyquist frequency, which means that $N_x \Delta x \ge 2D$ and $N_y \Delta x \ge 2H$; equivalently,

$$s_u \le \frac{\lambda_{\min}}{2Dp_u}, \qquad s_v \le \frac{\lambda_{\min}}{2Hp_v} \tag{12}$$

For GAIA-2, with $\lambda_{\min} = 300$ nm, $D = 1.4$ m, $H = 0.5$ m, $p_u = (10\ \mu\text{m})/(46.67\ \text{m})$ and $p_v = (30\ \mu\text{m})/(46.67\ \text{m})$, we have $s_u \le 0.50004$ and $s_v \le 0.46670$. Choosing $s_u = s_v = 0.125$ thus satisfies the sampling condition with ample margin. The computed image is a periodic function in u and v with periods $N_x \Delta u$ and $N_y \Delta v$, respectively. Some distance from the image centre the diffracted intensity generally decreases as u^{-2} or v^{-2}; this means that in order to reach a relative accuracy of r in the computed intensity at distance $\pm u$ from the centre, one needs $N_x \Delta u > u r^{-1/2}$. For instance, 1 per cent accuracy within ± 10 pixels (typical maximum window size) with $s_u = 0.125$ requires $N_x > 800$. The *minimum* useful discretisation is therefore $N_x = 1024$, $N_y = 512$, which was used in the present computations. (One further trick for improving numerical accuracy is to reduce the complex amplitude in (9), for each subpupil of size $\Delta x \Delta y$, by a factor equal to the square root of the fraction of the subpupil area actually within the the pupil.)

The quasi-monochromatic optical PSF is obtained by averaging $P_\lambda^O(u,v)$ over a limited wavelength region, weighted by some function $R_m(\lambda)$:

$$P_m^O(u,v) = \frac{\int P_\lambda^O(u,v) R_m(\lambda)\,\mathrm{d}\lambda}{\int R_m(\lambda)\,\mathrm{d}\lambda} \tag{13}$$

In the Astro field $R_m(\lambda)$ ($m = 1 \ldots 5$) could be the response functions of the adopted BBP photometric system. Clearly the normalisation is preserved so that $\iint P_m^O(u,v) = 1$.

The optical transfer function O_m is obtained as the inverse Fourier transform of P_m^O:

$$O_m(f_x, f_y) = \iint_{-\infty}^{+\infty} P_m^O(u,v) \exp[i2\pi(f_x u + f_y v)]\,\mathrm{d}u\,\mathrm{d}v \tag{14}$$

where f_x, f_y are the spatial frequencies along and across scan, expressed in periods per radian. Note that $O_m(0,0) = 1$. Equivalently,

$$P_m^O(u,v) = \frac{1}{4\pi^2} \iint_{-\infty}^{+\infty} O_m(f_x, f_y) \exp[-i2\pi(f_x u + f_y v)]\,\mathrm{d}f_x\,\mathrm{d}f_y \tag{15}$$

The effective PSF (pixel-integrated, smeared by TDI and across-scan motion and MTF, etc.) is obtained as the convolution of the optical PSF $P_m^O(u,v)$ with the various spatial response functions (e.g. a rectangular function of width p_u for the along-scan pixel integration). By means of the convolution theorem this effective PSF is also given by

$$P_m(u,v) = \frac{1}{4\pi^2} \iint_{-\infty}^{+\infty} O_m(f_x, f_y) M(f_x, f_y) \exp[-i2\pi(f_x u + f_y v)]\,\mathrm{d}f_x\,\mathrm{d}f_y \tag{16}$$

where $M(f_x, f_y)$ is the total modulation fransfer function of the various spatial responses. (It is assumed that these response functions are all symmetric, so that the transfer function is real, i.e. without phase shift.)

Considering: 1. the along-scan pixel integration (rectangle of width p_u); 2. the along-scan TDI integration (rectangular of width p_u/n_p, where $n_p = 4$ is the number of phases per pixel); 3. the across-scan pixel integration (rectangle of width p_v); 4. the across-scan image motion during the CCD integration time τ (rectangular of width $\omega_{\mathrm{ac}}\tau$); and finally 5. the electronic pixel cross talk which is modelled as a bivariate normal distribution with standard widths σ_u and σ_v (which may depend both on wavelength and the size of the charge packet), we have:

$$M(f_x, f_y) = \mathrm{sinc}(\pi f_x p_u)\mathrm{sinc}(\pi f_x p_u/n_p)\mathrm{sinc}(\pi f_y p_v)\mathrm{sinc}(\pi f_y \omega_{\mathrm{ac}}\tau) \times \exp[-2\pi^2(\sigma_u^2 f_x^2 + \sigma_v^2 f_y^2)] \tag{17}$$

The numerical calculation of $P(u,v)$ uses the DFT in (10) forward ($s = +1$) and backward ($s = -1$), with the MFT function applied in between. The end result must be divided by $N_x N_y$ to preserve the normalisation $\iint P_m(u,v) = 1$. The PSF is more conveniently expressed, not as intensity per steradian, but per pixel, which is obtained through multiplication with $p_u p_v$.

The along-scan line-spread function (LSF) is obtained by summing the PSF across-scan and multiplying with s_v; similarly the across-scan LSF is obtained by summing the PSF along-scan and multiplying with s_u.

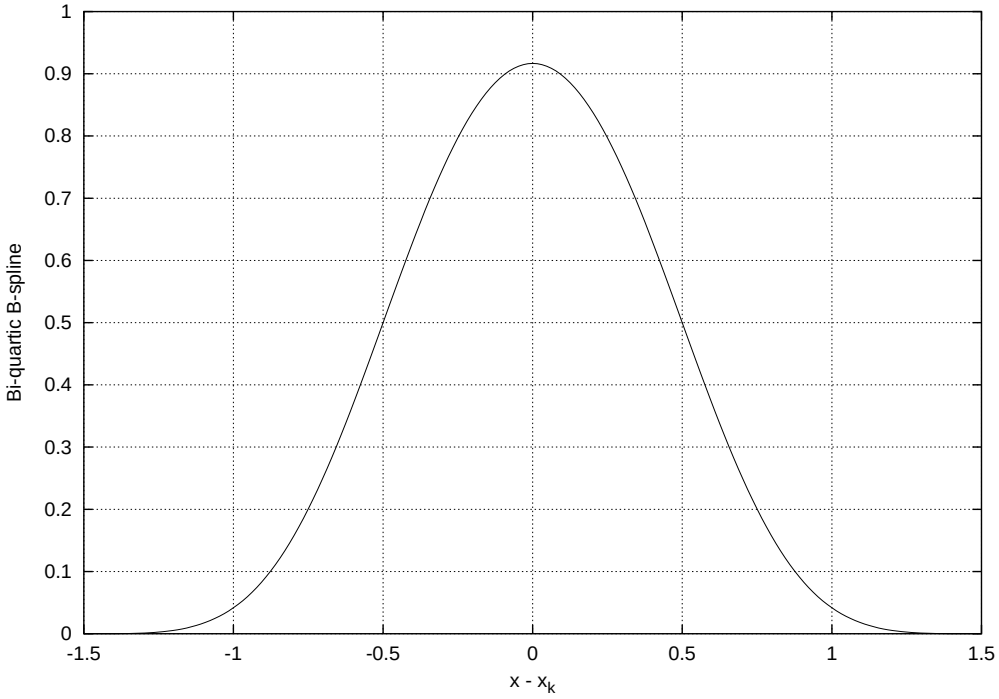

FIGURE 15: The bi-quartic B-spline $B_k(x)$.

Appendix B: The bi-quartic B-spline

The bi-quartic B-spline (both the concept and the name was invented for the present purpose) is obtained by adding two adjacent quartic B-splines on a regular knot sequence. We shall consider a knot sequence with interval 0.5, which is in principle infinite in both directions, thus $x_k = 0.5k + \delta$ for any integer k, where δ is a fixed number. The kth bi-quartic B-spline $B_k(x)$ is non-zero only in the interval $[x_{k-3}, x_{k+3}]$, i.e. for $x_k \pm 1.5$. It is normalised to unit area: $\int_{-\infty}^{+\infty} B_k(x)\,\mathrm{d}x = 1$.

An alternative way to define the bi-quartic B-spline is as follows: take a normalised cubic B-spline on the grid x_k, and convolve it with a centred, rectangular function of unit width and area. The last convolution guarantees that $\sum_j B_k(j-c) = 1$ for any c. Evidently the same holds for any linear combination $\sum_k b_k B_k(x)$ provided that $\sum_j b_j = 1$.

With $z = |x - x_k|$ we have (Fig. 15)

$$B_k(x) = \begin{cases} 0 & \text{if } \frac{3}{2} \le z \\ \frac{2}{3}(\frac{3}{2} - z)^4 & \text{if } 1 \le z < \frac{3}{2} \\ \frac{2}{3}(\frac{3}{2} - z)^4 - \frac{8}{3}(1-z)^4 & \text{if } \frac{1}{2} \le z < 1 \\ \frac{1}{12}(11 - 24z^2 + 16z^4) & \text{if } 0 \le z < \frac{1}{2} \end{cases} \tag{18}$$

Usually, however, in order to evaluate a function such as $f(x) = \sum_k b_k B_k(x)$, or to fit such

a function to given data, one needs to know the values of all non-zero B-splines at a given coordinate x. If $x_k \le x < x_{k+1}$, then one needs the six values $B_\ell(x)$, $\ell = k-2 \ldots k+3$. The subroutine `bqspl` shown below (based on de Boor) calculates these values, as well as the derivatives with respect to x, in a stable and efficient manner.

```
c**********************************************************************
      SUBROUTINE bqspl(z, bq0, bq1)
c**********************************************************************
c
c  For z = x-x_k between 0 and 0.5 (inclusive), this
c  subroutine returns the six non-zero bi-quartic
c  B-spline values B_l(x) (l = k-2 to k+3) in bq0(1:6),
c  and their derivatives wrt z in bqs1(1:6).
c  [LL 2003-04-29]
c
      REAL*8 z, bq0(6), bq1(6)
      INTEGER i, j
      REAL*8 s0, t0, s1, t1, deltal(5), deltar(5), dr, dl
      bq0(1) = 1.0
      bq1(1) = 0.0
      DO  j = 1, 4
          deltar(j) = 0.5*j - z
          deltal(j) = z - 0.5*(1-j)
          s0 = 0.0
          s1 = 0.0
          DO  i = 1, j
              dr = deltar(i)
              dl = deltal(j+1-i)
              t0 = bq0(i)/(dr + dl)
              t1 = bq1(i)/(dr + dl)
              bq0(i) = s0 + dr*t0
              bq1(i) = s1 - t0 + dr*t1
              s0 = dl*t0
              s1 = t0 + dl*t1
          ENDDO
          bq0(j+1) = s0
          bq1(j+1) = s1
      ENDDO
      bq0(6) = bq0(5)
      bq1(6) = bq1(5)
      DO  j = 5, 2, -1
          bq0(j) = bq0(j) + bq0(j-1)
          bq1(j) = bq1(j) + bq1(j-1)
      ENDDO
      RETURN
      END
```